

Supporting Information for

Mesoscale Nanoparticles Selectively Target the Renal Proximal Tubule Epithelium

Ryan M. Williams^a, Janki Shah^a, Brandon D. Ng^a, Denise R. Minton^b, Lorraine J. Gudas^c, Christopher Y. Park^{a,d}, Daniel A. Heller^{a,c*}

^aMemorial Sloan Kettering Cancer Center, New York, NY, USA

^bWeill Cornell Graduate School of Medical Sciences, New York, NY, USA

^cDepartment of Pharmacology, Weill Cornell Medical College, New York, NY, USA

^dDepartment of Cell and Developmental Biology, Weill Cornell Medical College, New York, NY, USA

*Contact: hellerd@mskcc.org; (646)888-3438

Supplementary Figures and Tables

Table S1. Nanoparticle biodistribution literature survey. A brief literature survey was conducted to investigate the effects of nanoparticle size and opsonization potential on biodistribution. Papers which studied nanoparticle biodistribution without the use of molecular targeting moieties were selected. Studies performed in diseased animals were excluded in order to determine biodistribution in healthy, uncompromised mice or rats. Only nanoparticles administered intravenously were included. The nanoparticle diameter, surface functionalization, and primary site of localization were recorded from each paper. Of papers containing many nanoparticles with minor size iterations, one representative particle was chosen. The opsonization potential of each particle was assigned a score with 1 being the most opsonizing and 5 being the least opsonizing. Category binning was performed as follows: 1- PLGA or gold particles with no coating; 2- Relatively opsonizing proteins, small molecule labels, or polymers (as described in the reference); 3- Relatively non-opsonizing protein or polymer (as described in the original manuscript); 4- PEG-coated particles with surface charge $-15 < X > +15$; 5- PEG-coated particles with surface charge $-15 > X < +15$ or non-opsonizing lipid (as described in the reference). Each cited nanoparticle was assigned a number (table below). The size and assigned degree of opsonization (surface category) were plotted for each referenced nanoparticle (Figure 1). The nanoparticles studied in this paper are the last four entries listed at the bottom of the table.

Type of Particle	Surface Coating	Primary Localization	Size (nm)	Opsonization Score	Particle #	Reference #
PLGA	None	Spleen	105	1	1	¹
PLGA	None	Spleen	160	1	2	¹
Gold-Apotransferrin	Apotransferrin	Liver	5	3	3	²
Lipid/Protein	Apolipoprotein	Kidney	25	5	4	³
PLGA	None	Liver	187	1	5	⁴
PLGA	mPEG 5000	Liver	67	5	6	⁵
PLGA	None	Liver	134	1	7	⁵
Gold50	mPEG 5000	Liver	79	5	8	⁶

PLGA	PEG 3400	Liver	150	4	9	⁷
Gold	PEG	Liver	10	4	10	⁸
Gold	PEG	Spleen	30	4	11	⁸
Gold	None	Liver	50	1	12	⁹
Gold	None	Liver	100	1	13	⁹
Gold	None	Liver	250	1	14	⁹
Silica	Radiolabel	Spleen	18	2	15	¹⁰
Silica	Fluorescent Dye	Liver	18	2	16	¹⁰
Iron Oxide	Starch	Spleen	104	2	17	¹¹
Iron Oxide	mPEG	Spleen	142	4	18	¹¹
Iron Oxide	mPEG	Spleen	169	4	19	¹¹
Vinylpyrrolidone 100: N-isopropylacrylamide 0	None	Liver	35	2	20	¹²
Vinylpyrrolidone 50: N-isopropylacrylamide 50	None	Liver	45	2	21	¹²
Radio labeled chitosan	Chitosan	Stomach	70	3	22	¹³
PLA	mPEG	Lymph Node	70	5	23	¹⁴
PLGA	None	Liver	214	1	24	¹⁵
PLGA	mPEG 5000	Liver	198	4	25	¹⁵
PLA	Poloxamer 188	Liver	136	4	26	¹⁶
PLA	PEG20k (10%)	Liver	176	4	27	¹⁶
PBAE	Pluronic F108	Kidney	113	4	28	¹⁷
PCL	Pluronic F108	Liver	200	4	29	¹⁷
Doxil (Liposome)	PEG	Liver	87	4	30	¹⁸
Iron Oxide	Pluronic F127	Spleen	86	3	31	¹⁹
Lipid	Lecithin	Spleen	197	2	32	²⁰
PLGA	PEG-carboxylic acid	Kidney	386	4	(-)	
PLGA	PEG-carboxylic acid-DMAB	Kidney	432	4	(+)	
PLGA	methoxy PEG	Kidney	328	5	(★)	
PLGA	None	Hepatobiliary	327	1	(○)	

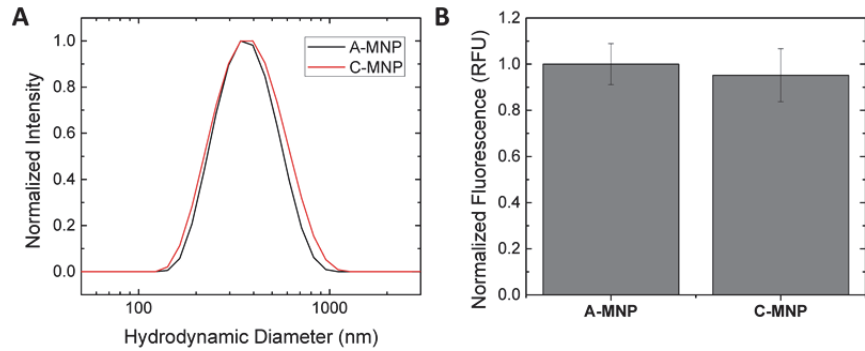


Figure S1. Nanoparticle size and fluorescence characterization. A) Normalized intensity distribution of nanoparticle diameter as measured by dynamic light scattering (DLS). B) Normalized fluorescence from an equal weight of each nanoparticle formulation.

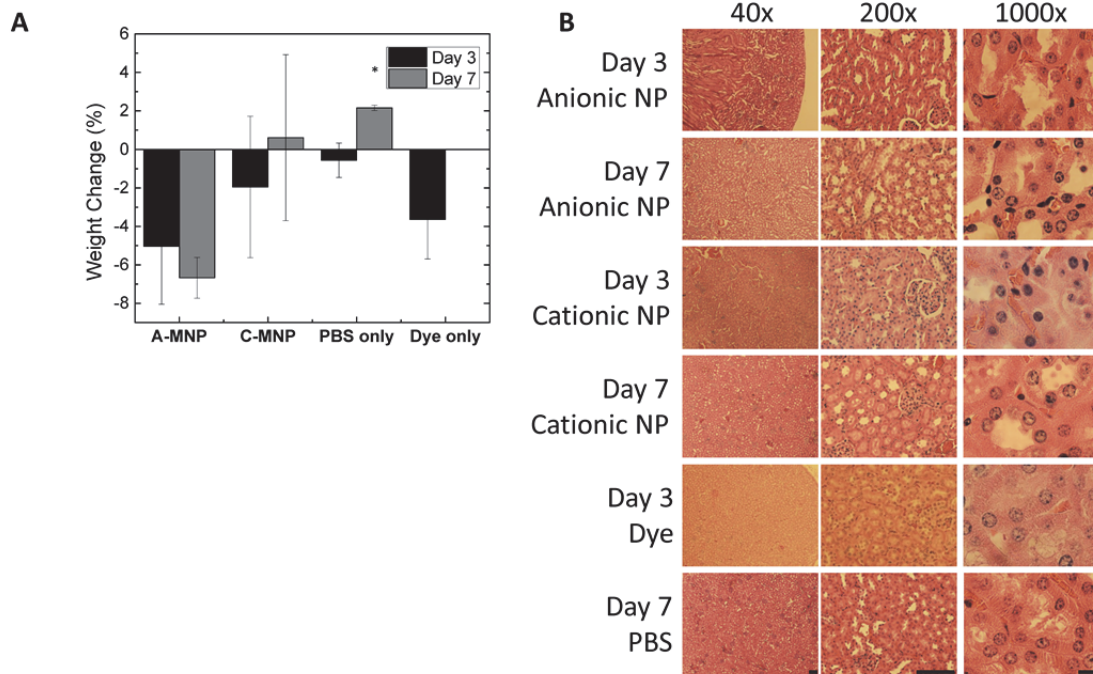


Figure S2. Mesoscale nanoparticle (MNP) toxicity studies. A) Percent change in weight from injection to day 3 or day 7 for mice with the given treatment (Mean \pm SD) (*= $p<0.05$). B) H&E stained renal tissue from mice with the noted treatment on the given day. Scale bar for 40x column: 10 μ m; 200x column: 100 μ m; 1000x column: 100 μ m.

Neither mice treated with anionic (A-MNP) nor cationic mesoscale nanoparticles (C-MNPs) exhibited a significant weight change at day 3 or day 7 compared to dye alone-treated mice after 3 days (Figure S2a). There was a significant weight increase in mice treated with PBS control at day 7 compared to dye alone. Therefore, any negative effects on mouse weight due to the nanoparticles may also be attributed to the dye, suggesting that MNPs themselves do not induce additional toxicity. The kidneys of mice treated with either MNP formulation showed no histomorphological evidence of damage after 3 or 7 days (Figure S2b). Haematoxylin/eosin stained slides were reviewed by a board-certified anatomic pathologist.

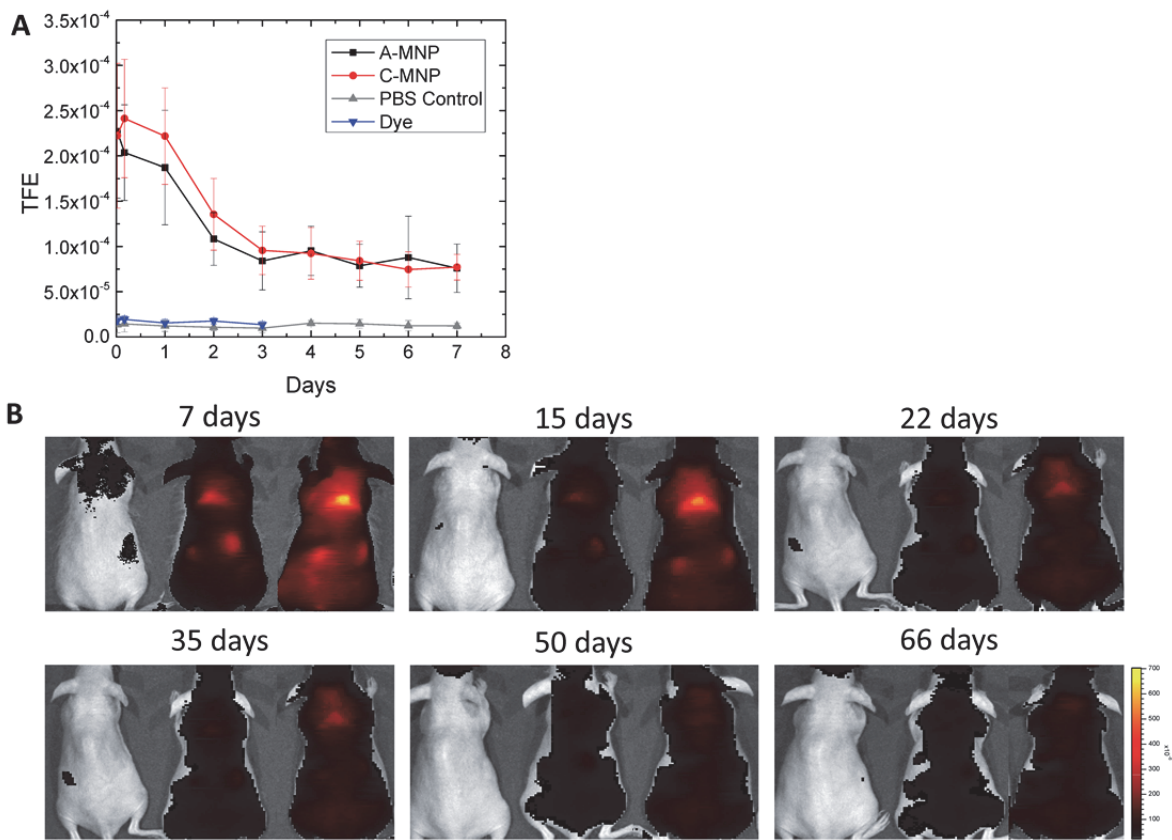


Figure S3. MNP fate in vivo. A) Nanoparticle fluorescence measured from the kidney region of live mice measured daily for 7 days after injection (Mean \pm SD). B) Fluorescence from nanoparticles in mice treated with (L to R): PBS, A-MNP, and C-MNP, measured up to 66 days after injection.

Mice treated with either A- or C-MNPs exhibited brighter fluorescence from the kidneys than mice treated with PBS alone or dye alone at all time points (Figure S3a). Fluorescence intensity decreased rapidly until approximately the third day following injection and then attenuated slowly thereafter. Fluorescence in the kidney region was visible for approximately 2 months following injection (Figure S3b). This pattern of nanoparticle degradation appears consistent with other reports of slow degradation of PLGA in vivo.^{21, 22}

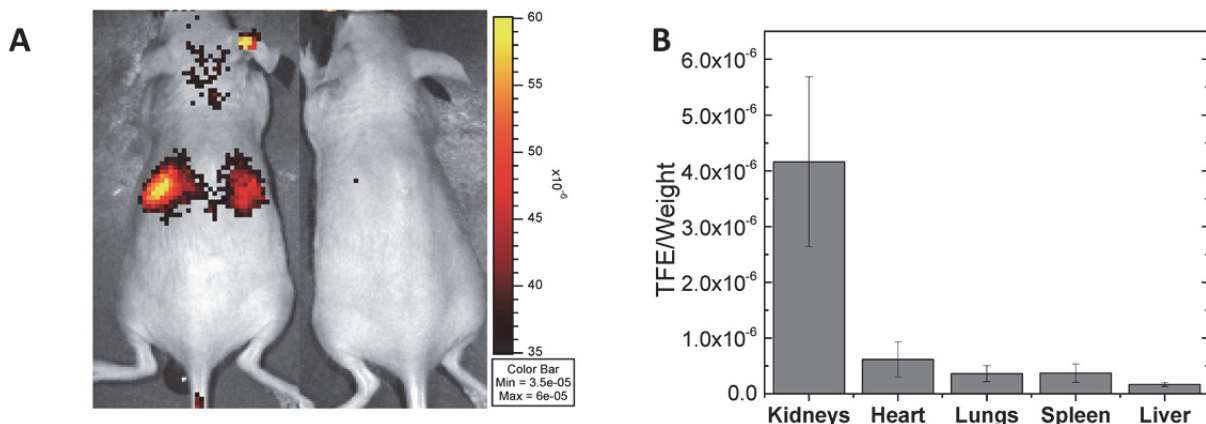


Figure S4. Distribution of neutral mesoscale nanoparticles (N-MNPs) injected into mice. A) In vivo fluorescence image acquired 30 minutes following injection. The mouse on the left was treated with 50 mg/kg N-MNPs. The mouse on the right was treated with PBS. B) Ex vivo fluorescence of each organ was normalized by dividing total fluorescence by organ weight (Mean \pm SD). p<0.05 for kidneys versus each organ.

Neutral PLGA mesoscale nanoparticles (N-MNPs) functionalized with a methoxy PEG surface were synthesized to encapsulate 0.23 μ g of DEDC dye per 1 mg of nanoparticle. The diameter of the resulting nanoparticles averaged 328.1 ± 5.3 nm with a ζ potential of 0.38 ± 0.70 mV. In vivo, they showed a similar biodistribution profile to both A- and C-MNPs. N-MNP accumulation in the kidneys was far greater than in other organs (Figure S4a). Ex vivo kidney fluorescence was 6.7 times higher than the heart, the second brightest organ (Figure S4b).

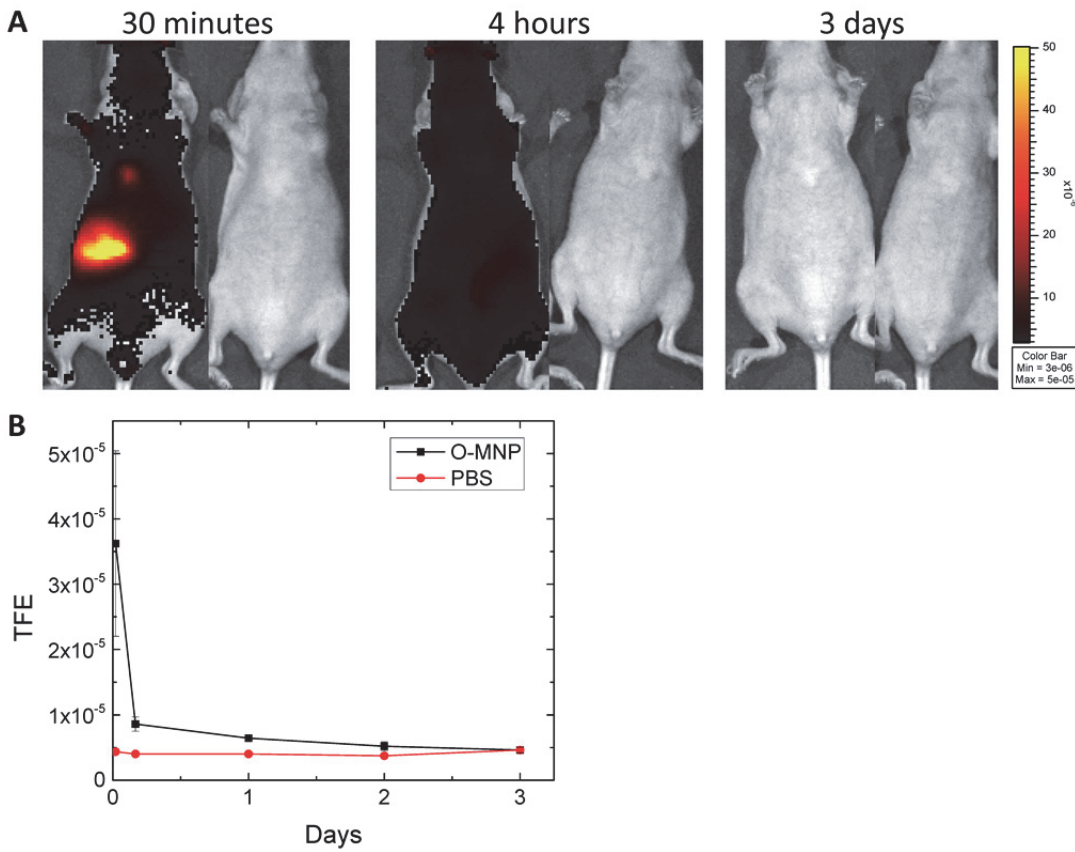


Figure S5. Localization of opsonizing PLGA nanoparticles synthesized without PEG (O-MNPs). A) In vivo fluorescence images of mice imaged ventrally at 30 minutes, 4 hours, and 3 days after injection of O-MNPs (left) and PBS (right). B) Quantification of in vivo liver fluorescence (Mean \pm SD for treated mice).

Opsonizing PLGA nanoparticles without PEG (O-MNPs), loaded with IR783 dye, localized in the liver 30 minutes following injection (Figure S5a). Four hours following injection, the signal in the liver disappeared, while low-level signal appeared in the intestines, suggesting hepatobiliary clearance of the nanoparticles. This experiment is consistent with studies showing that PLGA nanoparticles without PEG or other “stealth” moieties are endocytosed by liver Kupffer cells shortly after injection.²³⁻²⁶ Total fluorescence dissipated by 1 day post-injection and was absent at 3 days (Figure S5b). This experiment supports a model in which a non-opsonizing surface is necessary to avoid rapid uptake by the mononuclear phagocyte system (MPS) allowing targeting of non-MPS organs.

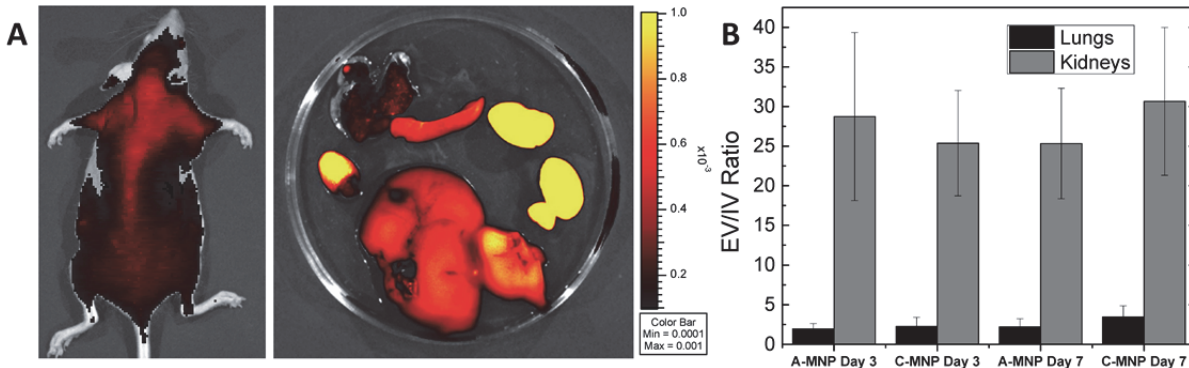


Figure S6. Comparison of ex vivo to in vivo fluorescence. A) Left: Emission from mouse carcass after removal of major organs. Right: Emission from organs removed from the mouse. From top center, clockwise: spleen, left kidney, right kidney, liver, heart, lungs. B) Ex vivo to in vivo ratio of fluorescence from lungs or kidneys of mice imaged at day 3 or 7 with A-MNPs or C-MNPs (Mean \pm SD).

The difference in nanoparticle fluorescence emission intensity between organs in vivo and ex vivo was assessed. One mouse, treated with 50 mg/kg A-MNPs, was euthanized 2 days following injection. In vivo, prior to euthanization, the fluorescence localization pattern was identical to that shown in similar experiments with the same treatment (Figure 3a, Figure S3b). After euthanizing and extracting organs, the carcass lacked bright foci, confirming that the fluorescence emanated from the removed organs (Figure S6a). Furthermore, the fluorescence in the kidneys ex vivo was brighter than all other organs, as we saw previously (Figure 3b). Additionally, the ex vivo signal from each kidney was 25-30 times higher than the signal in vivo, but this phenomenon was not seen in the lungs, which was only 2.0-3.5 times higher ex vivo than in vivo (Figure S6b). This phenomenon has been noted in the literature.²⁷

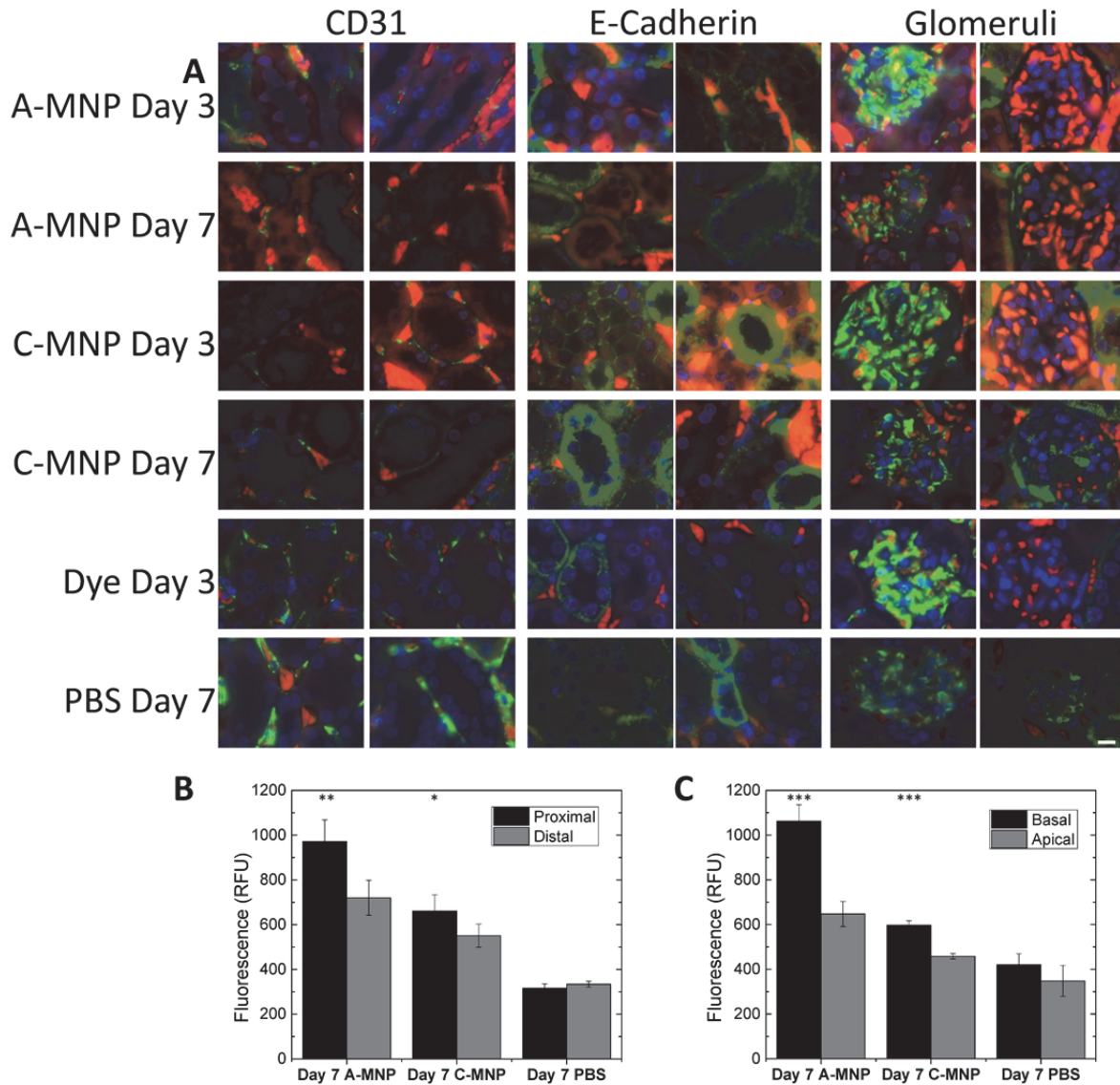


Figure S7. A) Representative micrographs of renal immunofluorescence. Images were acquired from mouse tissues at day 3 and day 7 after MNP injection. Blue = DAPI stain for cell nuclei, red = fluorescence from nanoparticles (excluding bright red blood cells which exhibit uniform autofluorescence), and green = either CD31 (left 2 columns) or E-Cadherin staining (center 2 columns). Images from glomeruli are also shown (right 2 columns) with CD31 staining on the left and E-Cadherin staining on the right. Scale bar denotes 10 μ m. (Note: The green signal intensities from CD31 and E-Cadherin stains were generated from different exposures and brightness levels, while all blue and green fluorescence signals were generated from identical exposures and brightness levels.) B) Fluorescence quantification in proximal versus distal tubules for each treatment at day 7. H) Fluorescence quantification in the basal portion of tubule epithelial cells versus the apical membrane at day 7 (Mean \pm SD). ***: $p < 0.001$; **: $p < 0.01$; *: $p < 0.05$.

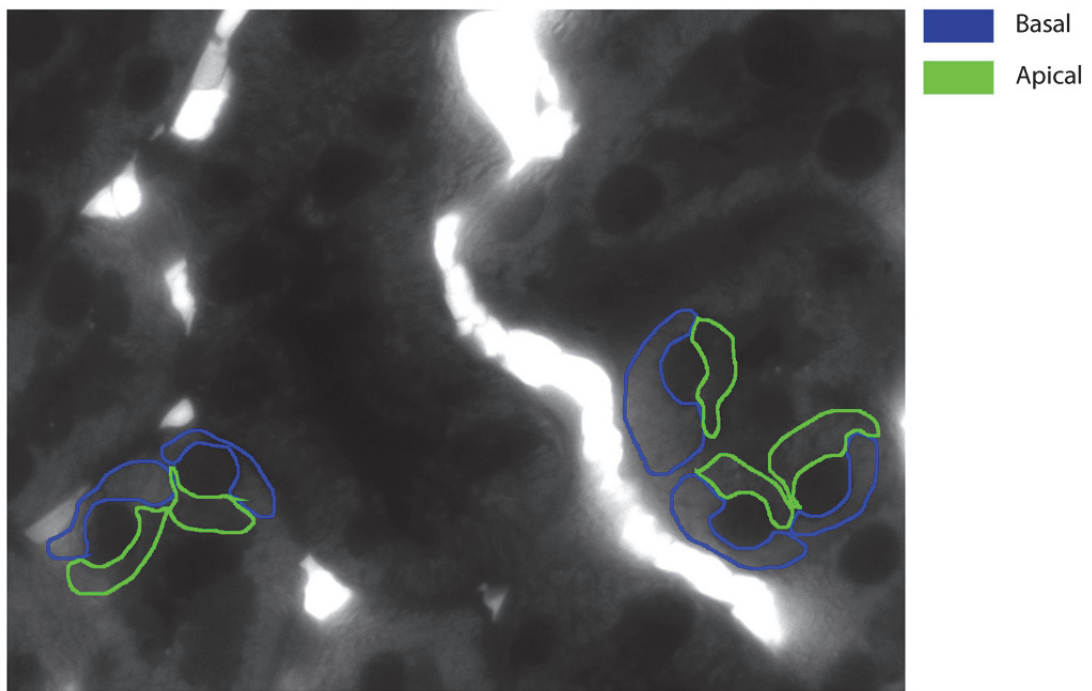


Figure S8. Selection of basal and apical portions of tubular epithelial cells for image quantification. The overlaid sections were selected from the Cy5 channel images in ImageJ. The representative image shown is that from Figure 3a “Cationic NP” image. This method was used for Figure 4h and S7b,c.

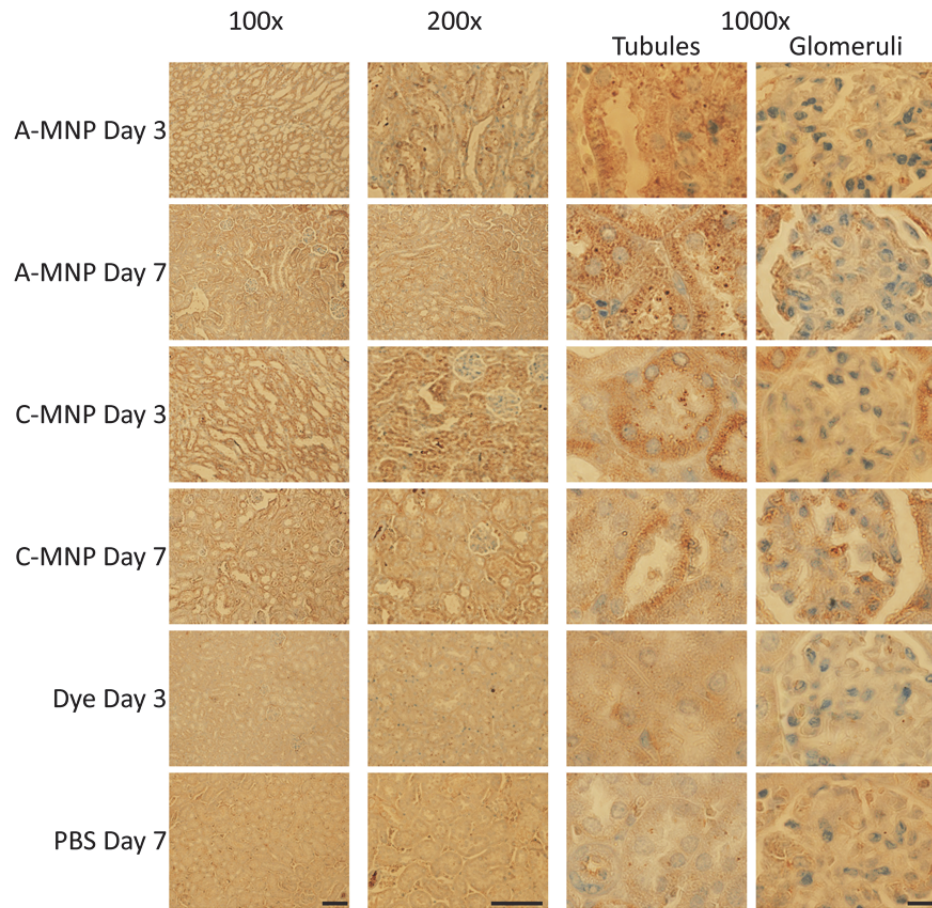


Figure S9. Immunohistochemical stains of renal tissue with anti-PEG antibody. Images of each group were taken with 10x, 20x, and 100x objectives to generate images with the indicated magnification. Scale bars are 100 μm for the 100x and 200x columns and 10 μm for the 1000x column.

Immunofluorescence and immunohistochemistry imaging of renal tissues from mice treated with A- or C-MNPs at day 7 revealed a similar basal staining pattern in the proximal tubules as on day 3 (Figure S7a, b, c, Figure S8, Figure S9).

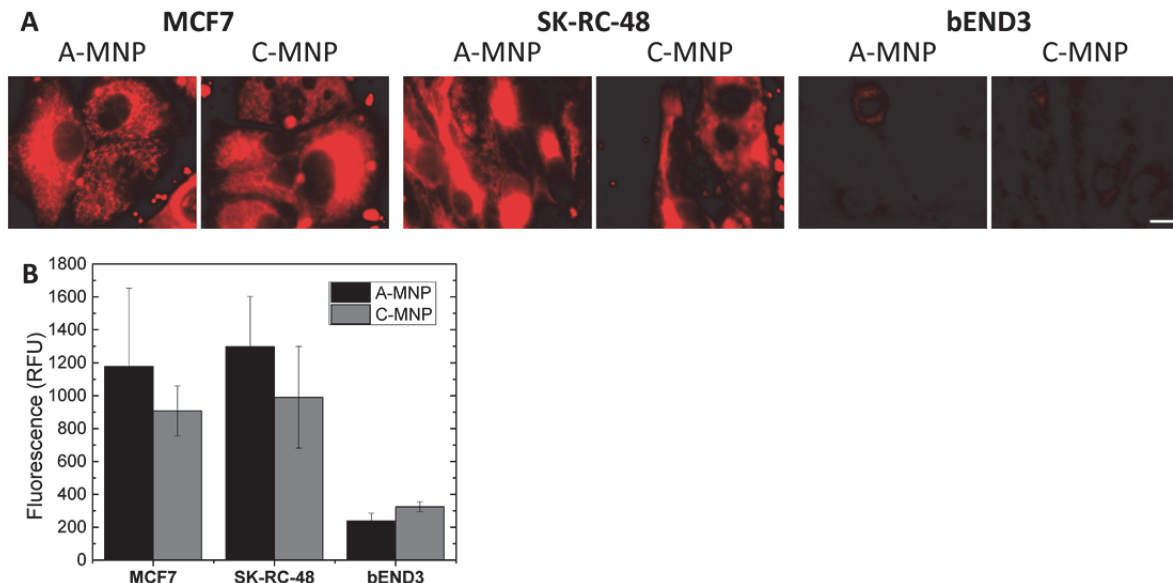


Figure S10. Mesoscale nanoparticle uptake in cell lines. A) Representative fluorescence images in three cell lines after a 10 minute incubation with A-MNPs or C-MNPs. B) Quantification of nanoparticle uptake in each cell line (Mean \pm SD). Scale bar is 10 μ m.

Fluorescence microscopy revealed uptake of MNPs in all three cell lines observed (Figure S10a). SK-RC-48 human clear cell renal cell carcinoma and MCF7 human breast adenocarcinoma cells exhibited strong emission of the encapsulated dye, while bEND.3 mouse brain endothelial cells showed lower emission (Figure S10b). Cells were also observed for approximately 48 hours following treatment; no significant cytotoxicity or loss of fluorescence was observed.

Materials and Methods

Nanoparticle Toxicity Study. Mice treated with A- or C-MNPs, dye alone, or PBS were weighed immediately preceding injection on the third day following treatment, and on the seventh day following treatment. The kidneys from mice in each group were sectioned as described in the Materials and Methods section in the main text. Sections were reviewed by a board-certified anatomic pathologist for histomorphological evidence of damage.

Long-Term In Vivo Biodistribution Study. Mice in each group were imaged using an IVIS Spectrum Pre-Clinical In Vivo Imaging System for 7 days as described in the main Materials and Methods. Separately, 3 mice, consisting of a mouse treated with PBS alone, A-MNPs, or C-MNPs were imaged every 1-2 weeks for approximately 3 months following injection to measure long-term fluorescence attenuation, which is interpreted to signify MNP degradation.

PLGA-methoxy PEG Nanoparticle Characterization. Neutral PLGA-mPEG mesoscale nanoparticles (N-MNPs) were synthesized and characterized essentially identically to PLGA nanoparticles functionalized with NH₂-PEG-COOH, which was described in the main text. Instead of using NH₂-PEG-COOH to synthesize the nanoparticles, however, NH₂-PEG-methoxy (MW 5kDa) (Nanocs; New York, NY) was conjugated to carboxylic acid-terminated PLGA. The resulting polymer was characterized by ¹H NMR as previously described.²⁸ Nanoparticles

encapsulating DEDC were formed with this polymer and characterized for size, ζ potential, and encapsulation as described in the main text.

A group of 3 SKH-1 Elite hairless mice were fed 5V75 chow for at least 1 week before the experiment to reduce fluorescent background from alfalfa-containing food. Mice were injected intravenously via the tail vein with 50 mg/kg of N-MNPs encapsulating DEDC for fluorescence localization studies. One control mouse was injected with 125 μ L PBS. These mice were imaged 30 minutes, 3 hours, and 1-3 days following injection with an IVIS Spectrum using 640 nm excitation and 680 nm emission filters. Total combined fluorescence efficiency from both kidneys was measured. At day 3, the mice were euthanized and the following organs were recovered, imaged, and weighed: kidneys, heart, lungs, spleen, and liver.

PLGA Nanoparticle Characterization. Opsonizing PLGA mesoscale nanoparticles (O-MNPs) were synthesized similarly to PLGA-PEG and PLGA-mPEG nanoparticles as described in the main text. Nanoparticles were formed by nanoprecipitation with PLGA and IR-783 fluorescent dye (25 mg used). The size, ζ potential, and encapsulation efficiency were measured. It should be noted that IR-783 was used instead of DEDC due to precipitate formation with the latter.

A group of 8 SKH-1 Elite hairless mice fed with 5V75 chow were injected intravenously via the tail vein with 50 mg/kg of O-MNPs encapsulating IR-783 for fluorescence localization studies. Two control mice were injected with 125 μ L PBS. These mice were imaged 30 minutes, 4 hours, and 24 hours following injection with the 647 nm excitation and 820 nm emission filters of an IVIS Spectrum. Four treated mice and one control mouse were euthanized after 24 hours. The remaining mice were imaged at 2 and 3 days following injection before sacrificing. Following euthanasia, the kidneys, heart, lungs, spleen, and liver were recovered, imaged, and weighed. Total fluorescence efficiency normalized by weight of each organ was obtained.

Ex Vivo to In Vivo Comparison. An SKH-1 Elite hairless mouse injected with 50 mg/kg A-MNPs was imaged via an IVIS Spectrum using the 650 nm excitation and 680 nm emission filters 2 days following injection. The mouse was euthanized and the kidneys, heart, lungs, spleen, and liver were extracted, leaving other organs intact and in place. The mouse without organs was then imaged as well as the organs alone.

To determine the difference in fluorescence from kidneys ex vivo versus in vivo, regions of interest (ROIs) were drawn around the kidneys and central lung region to obtain TFE for each ROI. After euthanasia and organ imaging, TFE was obtained for both kidneys and lungs. TFE for kidneys ex vivo was divided by that of kidneys in vivo to obtain the in vivo underestimation ratio. The same method was performed for the lungs.

In Vitro Nanoparticle Uptake. The following cell lines were used to determine the uptake of anionic and cationic nanoparticles in vitro: MCF-7 human breast adenocarcinoma (ATCC; Manassas, VA), SK-RC-48 human clear cell renal cell carcinoma (ccRCC) (Weill Cornell Medical College; New York, NY), and bEND.3 mouse brain endothelial cells (ATCC). MCF-7 cells were cultured in Dulbecco's Modified Eagle Medium (DMEM) with penicillin (10,000 U/mL), streptomycin (10,000 U/mL), glutamine (29.2 mg/mL) (Gibco; Carlsbad, CA), 0.01 mg/mL human recombinant insulin (Gibco), and 10% fetal bovine serum (FBS) (Gibco). SK-RC-48 cells were cultured in DMEM with 1X penicillin/streptomycin/glutamine and 10% FBS. bEND.3 cells were cultured in the same media as SK-RC-48 cells plus 1% glutaMAX

(Gibco). Cells were passaged approximately weekly and media was changed every 2-3 days. Cells were seeded into a 6-well cell culture dish for uptake studies. Stock suspensions of A-MNPs and C-MNPs in PBS were diluted with cell media to a final concentration of 100 µg/mL and incubated with each cell line for 10 minutes. Cells were washed with 2 x 1mL PBS before adding fresh media. Fluorescent images were captured 10 minutes following washing with the microscope and camera setup described in the main text, using Cy5 filters. Images were obtained with identical exposure times and processed using ImageJ software with identical brightness settings.

References

1. Yadav, K. S.; Chuttani, K.; Mishra, A. K.; Sawant, K. K. *PDA Journal of Pharmaceutical Science and Technology* **2011**, 65, 131-139.
2. Sun, C.; Yang, H.; Yuan, Y.; Tian, X.; Wang, L.; Guo, Y.; Xu, L.; Lei, J.; Gao, N.; Anderson, G. J. *J. Am. Chem. Soc.* **2011**, 133, 8617-8624.
3. Fischer, N. O.; Weilhammer, D. R.; Dunkle, A.; Thomas, C.; Hwang, M.; Corzett, M.; Lychak, C.; Mayer, W.; Urbin, S.; Collette, N. *PloS one* **2014**, 9, e93342.
4. Tosi, G.; Vergoni, A.; Ruozzi, B.; Bondioli, L.; Badiali, L.; Rivasi, F.; Costantino, L.; Forni, F.; Vandelli, M. *J. Controlled Release* **2010**, 145, 49-57.
5. Avgoustakis, K.; Beletsi, A.; Panagi, Z.; Klepetsanis, P.; Livaniou, E.; Evangelatos, G.; Ithakissios, D. *Int. J. Pharm.* **2003**, 259, 115-127.
6. Choi, C. H. J.; Zuckerman, J. E.; Webster, P.; Davis, M. E. *Proc. Natl. Acad. Sci.* **2011**, 108, 6656-6661.
7. Dhar, S.; Kolishetti, N.; Lippard, S. J.; Farokhzad, O. C. *Proc. Natl. Acad. Sci.* **2011**, 108, 1850-1855.
8. Zhang, X.-D.; Wu, D.; Shen, X.; Liu, P.-X.; Yang, N.; Zhao, B.; Zhang, H.; Sun, Y.-M.; Zhang, L.-A.; Fan, F.-Y. *International journal of nanomedicine* **2011**, 6, 2071.
9. De Jong, W. H.; Hagens, W. I.; Krystek, P.; Burger, M. C.; Sips, A. J.; Geertsma, R. E. *Biomaterials* **2008**, 29, 1912-1919.
10. Kumar, R.; Roy, I.; Ohulchanskky, T. Y.; Vathy, L. A.; Bergey, E. J.; Sajjad, M.; Prasad, P. N. *ACS nano* **2010**, 4, 699-708.
11. Cole, A. J.; David, A. E.; Wang, J.; Galbán, C. J.; Yang, V. C. *Biomaterials* **2011**, 32, 6291-6301.
12. Gaur, U.; Sahoo, S. K.; De, T. K.; Ghosh, P. C.; Maitra, A.; Ghosh, P. *Int. J. Pharm.* **2000**, 202, 1-10.
13. Banerjee, T.; Mitra, S.; Kumar Singh, A.; Kumar Sharma, R.; Maitra, A. *Int. J. Pharm.* **2002**, 243, 93-105.
14. Chaney, E. J.; Tang, L.; Tong, R.; Cheng, J.; Boppart, S. A. *Molecular imaging* **2010**, 9, 153.
15. Li, Y.-P.; Pei, Y.-Y.; Zhang, X.-Y.; Gu, Z.-H.; Zhou, Z.-H.; Yuan, W.-F.; Zhou, J.-J.; Zhu, J.-H.; Gao, X.-J. *J. Controlled Release* **2001**, 71, 203-211.
16. Mosqueira, V. C. F.; Legrand, P.; Morgat, J.-L.; Vert, M.; Mysiakine, E.; Gref, R.; Devissaguet, J.-P.; Barratt, G. *Pharmaceutical research* **2001**, 18, 1411-1419.
17. Shenoy, D.; Little, S.; Langer, R.; Amiji, M. *Pharmaceutical research* **2005**, 22, 2107-2114.
18. Bao, A.; Goins, B.; Klipper, R.; Negrete, G.; Phillips, W. T. *J. Pharmacol. Exp. Ther.* **2004**, 308, 419-425.

19. Jain, T. K.; Reddy, M. K.; Morales, M. A.; Leslie-Pelecky, D. L.; Labhsetwar, V. *Mol. Pharm.* **2008**, 5, 316-327.
20. Yang, S. C.; Lu, L. F.; Cai, Y.; Zhu, J. B.; Liang, B. W.; Yang, C. Z. *J. Controlled Release* **1999**, 59, 299-307.
21. Danhier, F.; Ansorena, E.; Silva, J. M.; Coco, R.; Le Breton, A.; Préat, V. *J. Controlled Release* **2012**, 161, 505-522.
22. Vert, M.; Mauduit, J.; Li, S. *Biomaterials* **1994**, 15, 1209-1213.
23. Gref, R.; Domb, A.; Quellec, P.; Blunk, T.; Müller, R.; Verbavatz, J.; Langer, R. *Adv. Drug Del. Rev.* **1995**, 16, 215-233.
24. Ogawara, K.-i.; Yoshida, M.; Higaki, K.; Kimura, T.; Shiraishi, K.; Nishikawa, M.; Takakura, Y.; Hashida, M. *J. Controlled Release* **1999**, 59, 15-22.
25. Panagi, Z.; Beletsi, A.; Evangelatos, G.; Livaniou, E.; Ithakissios, D.; Avgoustakis, K. *Int. J. Pharm.* **2001**, 221, 143-152.
26. Gref, R.; Minamitake, Y.; Peracchia, M. T.; Trubetskoy, V.; Torchilin, V.; Langer, R. *Science* **1994**, 263, 1600-1603.
27. Vasquez, K. O.; Casavant, C.; Peterson, J. D. *PLoS One* **2011**, 6, e20594.
28. Cheng, J.; Teply, B. A.; Sherifi, I.; Sung, J.; Luther, G.; Gu, F. X.; Levy-Nissenbaum, E.; Radovic-Moreno, A. F.; Langer, R.; Farokhzad, O. C. *Biomaterials* **2007**, 28, 869-876.

Movie Legend

Movie S1. A 3-dimensional reconstruction of combined fluorescence and computed tomography image of a mouse treated with A-MNPs.